Observation of Spin-Glass Behavior in Spinel Compound CoGa2O4

Jiyu Hu
Anhui University
Yongqing Ma (489364216@qq.com)
Anhui University https://orcid.org/0000-0002-0500-505X
Xucai Kan
Anhui University
Chaocheng Liu
Anhui University

Research Article

Keywords: SG behavior, FM-AFM competition, Magnetic frustration, AC susceptibility

Posted Date: February 19th, 2021

DOI: https://doi.org/10.21203/rs.3.rs-216990/v1

Abstract

In this work, the synthesis process, crystal-structure, and comprehensive physical properties of spinel compound $CoGa_2O_4$ have been investigated. The competition between antiferromagnetism (AFM) and ferromagnetism (FM) are considered to be the crucial elements for resulting in spin-glass (SG) behavior due to magnetic frustration. The observed SG behavior is determined by the temperature dependence of magnetization $M(T)$ curves under the ZFC (zero-field-cooled) and FCC (field-cooled) processes, where form the intense irreversibility divergence. Moreover, the corresponding fitting parameters (the freezing temperature T_0 = 9.32 K, the flipping time $\tau_0 = 4.49 \times 10^{-10}$ s, and the dynamical exponent zv = 4.46) strongly indicate the existence of the SG behavior. Meanwhile, as another specific characteristic for SG, in our present work, frequency (f) and magnetic field (H) have a strong influence on the peaks of AC susceptibility. From where, with the increase of f and H, the freezing temperature follows a corresponding peak shift. All the above phenomena and relevant analyses of magnetic frustration behavior confirm the typical SG behavior in $CoGa_2O_4$ system.

1. Introduction

Since the typical spin glass (SG) behavior has been found in magnetic materials, the sub-stable magnetic alloy material and magnetic compounds have been extensively studied due to its interesting structure and properties [1, 2]. The research of SG plays a crucial role in many comprehensive study of interdisciplines, meanwhile, it also provides mathematical tools to solve practical problems in memory elements, microwave components, computing machinery, functional materials, and biology science [3–5]. As is known to all, the SG behavior is usually existed in the antiperovskite compounds with a formula AXM_3 (A = Ga, Al, Cu, In, Sn, Zn, Ge etc.; X = C, N; M = Ni, Mn, Fe, etc) such as $SnCFe_3$ [6] and $GaNMn_3$ [7]. However, to date, there are no report on the SG behavior in $CoGa_2O_4$ spinel compound, and thus the work seems more necessary and meaningful.

In this paper, the spinel structure $CoGa_2O_4$ has been prepared by solid state method. The distribution of the cations at the tetrahedral and the octahedral sites can be reflected by the structural formula $(Co_{1-x}Ga_x)[Co_xGa_{2-x}]O_4$ [8, 9]. It can be seen that, Co^{2+} ions and Ga^{3+} ions are both divided into A and B-sites. We report and verify the spin glass behavior of the prepared sample, from where, the SG behavior in $CoGa_2O_4$ is confirmed to be resulted from the magnetic frustration and atomic disorders according to the systematical measurements. The temperature dependence of magnetization $M(T)$ and magnetic susceptibility $\chi(T)$ are measured at several fixed frequencies. The isothermal remanent magnetization (M_{IRM}) are also performed and described in the following sections. We illustrate a detailed investigation of the magnetic property and structural characteristic of the sample. As all results shown, the competition between AFM and FM interactions should be responsible for the SG behavior of $CoGa_2O_4$ [10, 11].

2. Experimental Details

$CoGa_2O_4$ with the chemical formula of $(Co_{1-x}Ga_x)[Co_xGa_{2-x}]O_4$ was analyzed by standard solid state reaction method in air atmosphere. The powder of materials Co_2O_3 (100%) and Ga_2O_3 (99.8%) were used as starting materials, and homogeneous mixed by the ball milling. The mixture was sintered at 1300 ℃ in the muffle for 12 h. When the sample is cooled to room temperature at a rate of 3 K/min, the sample is basically prepared. After quenching to room temperature, the products were pulverized, mixed, pressed into pellets, and annealed again in order to obtain homogeneous samples.

The phase identification of the prepared sample was measured by X-ray diffraction at room temperature (XRD, Rigaku D/max-2550V/PC, Cu Kα (λ = 1.5406 Å)) with the angle from 20° to 90°. Scanning electron microscope (SEM) was used to characterize the microstructure, and Energy Dispersive X-Ray spectroscopy (EDX) was used to analyze the element composition. All the magnetic measurements were performed by a Quantum Design superconducting quantum interference device based on magnetic property measurement system (SQUID-MPMS 3).

3. Results And Discussion

Figure 1. (a) XRD spectra and Rietveld refinement at room temperature for $CoGa_2O_4$. Inset shows the Rietveld refinement XRD pattern. (b) The crystal structure of $CoGa_2O_4$.

In order to further gain the insight of element composition and state of $CoGa_2O_4$, XPS spectrum of the sample is illustrated in Fig. 3. Figure 3(a) presents the survey XPS spectrum of $CoGa_2O_4$ sample, where the survey XPS spectrum contains the peaks of O 1s, Ga 2p, and Co 2p, and confirms the existence of Co, Ga, and O in the $CoGa_2O_4$ composite. As shown in Fig. 3(b), the Co 2p spectrum is exhibited, in which the binding energies of the Co $2p_{1/2}$ and Co $2p_{3/2}$ have four peaks at 803.2 eV, 797 eV, 786.6 eV, and 781.3 eV. Meanwhile, two specific peaks at 781.3 eV and 797 eV are attributed to Co^{3+}, and the other two peaks at 786.6 eV and 803.2 eV are associated with Co^{2+} [18–20]. Figure 3(c) shows the XPS spectrum of Ga 2p. The observed energy peaks of Ga $2p_{1/2}$ and Ga $2p_{3/2}$ are located at 1144.5 eV and 1117.7 eV respectively [21, 22]. In the case of Fig. 3(d) for O 1s spectra, the peak with binding energy of 531.05 eV is related to oxygen bonding [23, 24]. Through the analyses above, all of the measurement results of XPS spectrum show that the prepared sample contains all the elements, which are well consistent with other related investigations.

Figure 4(a) shows the temperature dependence of magnetization *M(T)* curves for $CoGa_2O_4$ at different magnetic fields under the processes of zero field cooled (ZFC) and field cooled (FC). It is not difficult to identify that the compound adopts a characteristic of spin glass behavior since the M_{ZFC} and M_{FC} curves exhibit significant divergence at lower temperatures. The observed spin glass behavior of the sample may be due to the disorder of atoms and the competition of different magnetic spin-orders [25]. Meanwhile, with increasing the applied magnetic field, both the peak position of weak irreversibility T_{wi} (defined as the temperature where $M_{ZFC} = M_{FC}$) and strong irreversibility T_{si} (defined by the maximum value of magnetization) curves shift to lower temperature. It is shown that the spin glass state is gradually

destroyed under a large external magnetic field [26]. As plotted in Fig. 4(a), an obvious irreversibility appears below T_{wi}, which are the typical characteristic of spin glass behavior. Below T_{wi}, the value of M_{FC} remains almost a constant, meanwhile, M_{ZFC} almost drops to zero as the temperature decreases. According to previous reports, at low temperature, the difference between M_{FC} and M_{ZFC} curves may be resulted from the competition between magnetic couplings [27]. As shown in Fig. 4(b), the magnetic hysteresis loops (*M-H*) for $CoGa_2O_4$ sample are performed at 300 K and 5 K respectively. All $M(H)$ curves have a linear relationship with magnetic field in high field, which is consistent with spin glass system. According to the obtained results, neither of them reach saturation even up to 50 kOe. For another prominent case, M is bigger than 300 K at 5 K because of thermal disturbance has a susceptible effect on the magnetic moment.

In order to further confirm the spin-glass behavior, we characterized the temperature dependence of AC magnetic susceptibility under the changing frequency and magnetic field process. Figure 5(a) and 5(b) display AC magnetic susceptibility $\chi(T)$ for $CoGa_2O_4$ at AC field of H_{AC} = 2 Oe under different fixed frequencies (f = 1, 10, 100, 500, and 1000 Hz), respectively. It can be found that both $\chi'(T)$ and $\chi''(T)$ present strongly frequency-dependent peaks, obviously, the positions of these peaks shift to higher temperatures and the magnitudes decrease with increasing f, which indicate a typical spin glass behavior. Generally, $\Delta T_f/[T_f\Delta(\log_{10}f)]$ can determine the dependence of peak shift on frequency, and the typical value for spin-glass system is between 0.0045 and 0.08. Under the AC magnetic field, the energy of the applied magnetic field becomes smaller in one direction, and H_{AC} changes rapidly in the opposite direction with the increase of f. Meanwhile, the system needs a higher temperature field $T_f(f)$ to reach a stable state. In fact, the value of relaxation time τ around the transition temperature can be written as follows [28]:

$$\tau = \tau_0[T_f(f)/T_0\text{-}1]^{-zv},\ T_f > T_0 \quad (1)$$

Here, T_0 represents the freezing temperature, τ stands for the relaxation time $\tau = 1/(2\pi f)$, τ_0 stands for the characteristic flipping time of the magnetic moments, T_f is the frequency dependent of the peak position in $\chi'(T)$, and zv is the dynamical critical exponent. Acknowledged from the previous reports on spin glass, the parameters of τ_0 and zv for typical spin glass are located as follows, where τ_0 is in the range of 10^{-10}-10^{-13} s and zv is 4–13, respectively. In this paper, the parameters of T_0 = 9.32 K, $\tau_0 = 4.49\times10^{-10}$ s, and zv = 4.64 obtained by fitting formula (1) further suggest the typical spin-glass behavior [6]. Figure 5(c) and 5(d) present the $\chi'(T)$ and $\chi''(T)$ for $CoGa_2O_4$ under several bias DC magnetic fields respectively, with AC magnetic field H_{AC} = 2 Oe and f = 10 Hz. It is clearly shown that the values of T_f transfer to a lower temperature and the value of peak decreases with H_{DC} increase. There is a typical dependence and linear relationship between the value of $T_f(H)$ and $H^{2/3}$, which is expected for the 3D-Heisenberg SG behavior [29].

The isothermal remanent magnetization $M_{IRM}(t)$ was measured under ZFC process with different magnetic fields from 300 to 5 K. It is necessary to emphasize the measurement process that under the premise of cooling the sample to the required temperature in the zero field, then apply a magnetic field for about 600 s and measure the remanent magnetization with decaying time. It is obviously seen from the Fig. 6 that M_{IRM} is mainly a straight line and is nonzero in different fields, which proves the distinct existence of spin frustration in $CoGa_2O_4$ and also a typical SG behavior. The data of experiment under different fields can be obtained by fitting the following formula [28, 30]:

$$M_{IRM}(t) = M_0 - a\ln(t), \quad (2)$$

As shown in the inset of Fig. 6, the relationship between fitting parameters M_0 and a is depicted. Obviously both parameters increase rapidly and then tend to saturate, which further proves the SG behavior of $CoGa_2O_4$ [31, 32].

In Fig. 7, we have exhibited PODS and total DOS for spin-up (↑) and spin-down (↓) states for $CoGa_2O_4$ and the figure is formed by the s, p, d and Total states. It can be concluded from the figure that the conduction band in $CoGa_2O_4$ is about 15 eV wide and is formed by the Co 3d states, Ga 4s, 4p states and O 2p states. The width of the valence band is about 15 eV and consists of two sub-band, it is also clear in the band structure: the one between − 8 and 0 eV is the O 2p states and Co 3d states. The other one is between − 15 and − 13 eV is created by Co 3d states. The band between − 20 and − 18 eV is due to the Ga 4s states [33]. The spin magnetic moments of the spin up and spin down with asymmetric distribution imply the net magnetization in the sample [28]. The calculated magnetic characteristics of $CoGa_2O_4$ are consistent with the measured magnetic properties.

We note that the $CoGa_2O_4$ sample also behaves a SG behavior with the reliable parameters: $\Delta T_f/[T_f\Delta(\log_{10} f)] \sim 0.025$, $T_0 = 9.32$ K, $\tau_0 = 4.49\times10^{-10}$ s, and $zv = 4.64$. As the result shown that the characteristic parameter varying with the different fixed frequencies: the magnitude of $\Delta T_f/[T_f\Delta(\log_{10} f)]$ decreases with increasing f, which indicates a strong dependence on frequency and associates with a typical SG behavior in $CoGa_2O_4$. Generally, the existence of SG is closely associated with the competition between FM and AFM interactions which results from the multiconfiguration of spins or spin frustration. The similar case have been reported in other analogous spinel ferrites as well as antiperovskite compounds [$Zn_{0.8-x}Ni_xCu_{0.2}Fe_2O_4$ and $SnNCo_3$] [1, 28], where the local FM cluster and atomic disorder caused by the atomic deficiency were observed. And thus, based on these discussions, the origin of SG behavior in our present work should be closely dependent upon the spin frustrations and disorder occupations of the mixed sites. That is to say, the observed SG behavior in $CoGa_2O_4$ may be attributed to the atomic disorders introduced by the Ga/Co deficiency which affects the characteristic parameters of the SG state remarkably.

4. Conclusion

In summary, the structure and magnetic properties of the compound $CoGa_2O_4$ were investigated systematically. The results of XRD, EDX, and XPS confirmed that the pure $CoGa_2O_4$ sample was prepared, and exhilaratingly, SG was also observed in $CoGa_2O_4$ from magnetic measurements. To further elaborate the SG, the following work is completed, for instance, $M(T)$ curves with different applied field/frequency, field dependent AC susceptibility, and M_{IRM} at fixed magnetic fields. The characteristic parameters T_0 = 9.32 K, $\tau_0 = 4.49\times10^{-10}$ s, and $zv = 4.64$ obtained from AC magnetic susceptibility indicate that $CoGa_2O_4$ is a SG system. Meanwhile, the curves of $M(T)$, $\chi'(T)$, and $\chi''(T)$ change regularly with the variation of magnetic and frequency. These phenomena can be explained by different magnetic competition and disorder. In other words, the competition between FM and AFM leads to the existence of SG, which is characterized by spin frustration and disorder. On this basis, the spin glass behavior of $CoGa_2O_4$ may be also caused by the competition between competing magnetic orders.

Declarations

Acknowledgment

The authors acknowledge the financial supported by the National Natural Science Foundation of China (Grant Nos. U19A2093 and 51802002) and the open fund for Discipline Construction, Institute of Physical Science and Information Technology, Anhui University.

Data Availability

All data generated or analyzed during this study are included in this published article.

Compliance with ethical standards

Conflict of interest The authors declare that they have no known competing financial interests or personal relationships that could have appeared to influence the work reported in this paper.

References

1. W. Yang, X.C. Kan, X.S. Liu, Z.Z. Wang, Z.H. Chen, Z. Wang, R.W. Zhu, M. Shezad, Spin glass behavior in $Zn_{0.8-x}Ni_xCu_{0.2}Fe_2O_4$ ($0 \leq x \leq 0.28$) ferrites. Ceram Int. 45, 23328-23332 (2019)
2. K.F. Wang, Y. Wang, L.F. Wang, S. Dong, Cluster-glass state in manganites induced by A-site cation-size disorder. Phys Rev B. 73, 134411 (2006)
3. S. Mahana, D. Topwal, Complex spin glass behavior in $Ga_{2-x}Fe_xO_3$. Appl Phys Lett. 110, 102907 (2017)
4. D.L. Stein, A model of protein conformational substates. Proc Natl Acad Sci. 82, 3670 (1985)
5. A.G. Hudetz, C.J. Humphries, J.R. Binder, Spin-glass model predicts metastable brain states that diminish in anesthesia. Front Syst Neurosci. 8, 234 (2014)

6. B.S. Wang, P. Tong, Y.P. Sun, X.B. Zhu, Z.R. Yang, W.H. Song, J.M. Dai, Observation of spin-glass behavior in antiperovskite compound $SnCFe_3$. Appl Phys Lett. 97, 042508 (2010)
7. J.C. Lin, P. Tong, D.P. Cui, C. Yang, S. Lin, W.J. Lu, B.S. Wang, B.C. Zhao, Y.P. Sun, Exchange bias induced after zero-field cooling in antiperovskite compounds $Ga_{1-x}NMn_{3+x}$. Phys Status Solidi B. 252, No. 3 (2015)
8. H.Y. Playford, A.C. Hannon, M.G. Tucker, M.R. Lees, R.I. Walton, Total neutron scattering investigation of the structure of a cobalt gallium oxide spinel prepared by solvothermal oxidation of gallium metal. J Phys Condens Matter. 25, 454212 (2013)
9. Z.H. He, J.F. Gao, L.B. Kong, Polycationic bimetallic oxide $CoGa_2O_4$ with spinel structure: dominated pseudocapacitance, dual-energy storage mechanism, and Li-ion hybrid supercapacitor application. Ionics. 26, 1379-1388 (2020)
10. L. Personnaz, I. Guyon, G. Dreyfus, Information storage and retrieval in spin-glass like neural networks. J Phys Lett. 46, 359 (1985)
11. L. Ding, C. Wang, Y. Sun, C.V. Colin, L.H. Chu, Spin-glass-like behavior and negative thermal expansion in antiperovskite $Mn_3Ni_{1-x}Cu_xN$ compounds. J Appl Phys. 117, 213915 (2015)
12. I. Mindru, D. Gingasu, G. Marinescu, L. Patron, L. Diamandescu, M. Feder, J.M. Calderon-Moreno, N. Stanica, Tartarate precursors to $Co_xZn_{1-x}Ga_2O_4$ spinel oxides. Mater Chem Phys. 134, 478-483 (2012)
13. H. Chen, G.D. Li, M.H. Fan, Q. Gao, J.B. Hu, S. Ao, C.D. Wei, X.X. Zou, Electrospinning preparation of mesoporous spinel gallate (MGa_2O_4; M=Ni, Cu, Co) nanofibers and their M(II) ions-dependent gas sensing properties. Sens Actuator B-Chem. 240, 689-696 (2017)
14. H. Li, C.X. Su, C.Q. Wang, Z. Lü, Electrochemical performance evaluation of $FeCo_2O_4$ spinel composite cathode for solid oxide fuel cells. J Alloy Compd. 829, 154493 (2020)
15. M.M. Can, T. Karaman, S. Shawuti, Optical and structural modification of boron-doped $CoGa_2O_4$ particles. Ceram Int. 46, 13025-13032 (2020)
16. X.Y. Hu, F.G. Li, D.M. Shi, Y. Xie, Z. Li, F.C. Yin, A design of self-generated Ti-Al-Si gradient coatings on Ti-6Al-4V alloy based on silicon concentration gradient. J Alloy Compd. 830, 154670 (2020)
17. A.H. Nassajpour-Esfahani, R. Emadi, A. Alhaji, A. Bahrami, M.R. Haftbaradaran-Esfahani, Towards high strength $MgAl_2O_4/Si_3N_4$ transparent nanocomposite, using spark plasma sintering. J Alloy Compd. 830, 154588 (2020)
18. Y.L. Zhai, Y.Z. Dai, J. Guo, L.L. Zhou, M.X. Chen, H.T. Yang, L.P. Peng, Novel biochar@$CoFe_2O_4/Ag_3PO_4$ photocatalysts for highly efficient degradation of bisphenol a under visible-light irradiation. J Colloid Interface Sci. 560, 111-121 (2020)
19. K. Zhang, D.D. Sun, C. Ma, G.L. Wang, X.L. Dong, X.X. Zhang, Activation of peroxymonosulfate by $CoFe_2O_4$ loaded on metal-organic framework for the degradation of organic dye. Chemosphere 241, 125021 (2020)

20. J.Y. Wang, Z. Yang, M.L. Zhang, Y.Q. Gong, Vertically stacked bilayer heterostructure $CoFe_2O_4$@Ni_3S_2 on a 3D nickel foam as a high-performance electrocatalyst for the oxygen evolution reaction. New J Chem. 44, 1455-1462 (2020)
21. D. Liu, X.P. Mo, K.X. Li, Y. Liu, J.J. Wang, T.T. Yang, The performance of spinel bulk-like oxygen-deficient $CoGa_2O_4$ as an air-cathode catalyst in microbial fuel cell. J Power Sources. 359, 355-362 (2017)
22. M. Kashif, M.H. Yuan, M. Abduallah, Y.X. Su, Fully selective catalytic oxidation of NO to NO_2 over most active Ga-PCH catalyst. J Environ Chem Eng. 8, 103524 (2020)
23. H.X. Zhang, L.C.Z. Neng, Y. Liu, Y.J. Gao, X.W. Cheng, Efficient removal of organic pollutant by activation of persulfate with magnetic Co_3O_4/$CoFe_2O_4$ composite. Arab J Chem. 13, 5332-5344 (2020)
24. Y.B. Zhang, J. Wang, Z.J. Su, M.M. Lu, S. Liu, F.Q. Gu, J.C. Liu, Y.K. Tu, T. Jiang, Spinel $MnFe_2O_4$ nanoparticles (MFO-NPs) for CO_2 cyclic decomposition prepared from ferromanganese ores. Ceram Int. 46, 14206-14216 (2020)
25. X.C. Kan, B.S. Wang, L. Zhang, L. Zu, S. Lin, J.C. Lin, P. Tong, W.H. Song, Y.P. Sun, Critical behavior in tetragonal antiperovskite $GeNFe_3$ with a frustrated ferromagnetic state. Phys Chem Chem Phys. 19, 13703-13709 (2017)
26. S. Karmakar, S. Taran, E. Bose, B.K. Chaudhuri, Evidence of intrinsic exchange bias and its origin in spin-glass-like disordered $L_{0.5}Sr_{0.5}MnO_3$ manganites (L=Y, $Y_{0.5}Sm_{0.5}$, and $Y_{0.5}La_{0.5}$). Phys Rev B. 77, 144409 (2008)
27. A. Malinowski, V.L. Bezusyy, R. Minikayev, P. Dziawa, Y. Syryanyy, M. Sawicki, Spin-glass behavior in Ni-doped $La_{1.85}Sr_{0.15}CuO_4$. Phys Rev B. 84, 024409 (2011)
28. C.C. Liu, X.Y.N. Tao, X.C. Kan, X.S. Liu, C.H. Zhang, S.J. Feng, Y.J. Yang, Q.R. Lv, J.Y. Hu, M. Shezad, Spin-glass behavior in Co-based antiperovskite compound $SnNCo_3$. Appl Phys Lett. 116, 052401 (2020)
29. S. Lin, D.F. Shao, J.C. Lin, L. Zu, X.C. Kan, B.S. Wang, Y.N. Huang, W.H. Song, W.J. Lu, P. Tong, Y.P. Sun, Spin-glass behavior and zero-field-cooled exchange bias in a Cr-based antiperovskite compound $PdNCr_3$. J Mater Chem C. 3, 5683-5696 (2015)
30. X.H. Zhang, Q. Yuan, J.C. Han, J.G. Zhao, J.K. Jian, Z.H. Zhang, B. Song, Observation of spin-glass behavior in antiperovskite compound $Mn_3Cu_{0.7}Ga_{0.3}N$. Appl Phys Lett. 103, 022405 (2013)
31. A. Aharoni, E.P. Wohlfarth, The isothermal remanence (IRM) and the thermoremanence (TRM) of spin glasses. J Appl Phys. 551664 (1984)
32. B. Song, J.K. Jian, H.Q. Bao, M. Lei, H. Li, G. Wang, Y.P. Xu, X.L. Chen, Observation of spin-glass behavior in antiperovskite Mn_3GaN. Appl Phys Lett. 92, 192511 (2008)
33. M.G. Brik, First-principles calculations of electronic, optical and elastic properties of $ZnAl_2S_4$ and $ZnGa_2O_4$. J. Phys. Chem. Solids. 71, 1435–14 42 (2010)

Figures

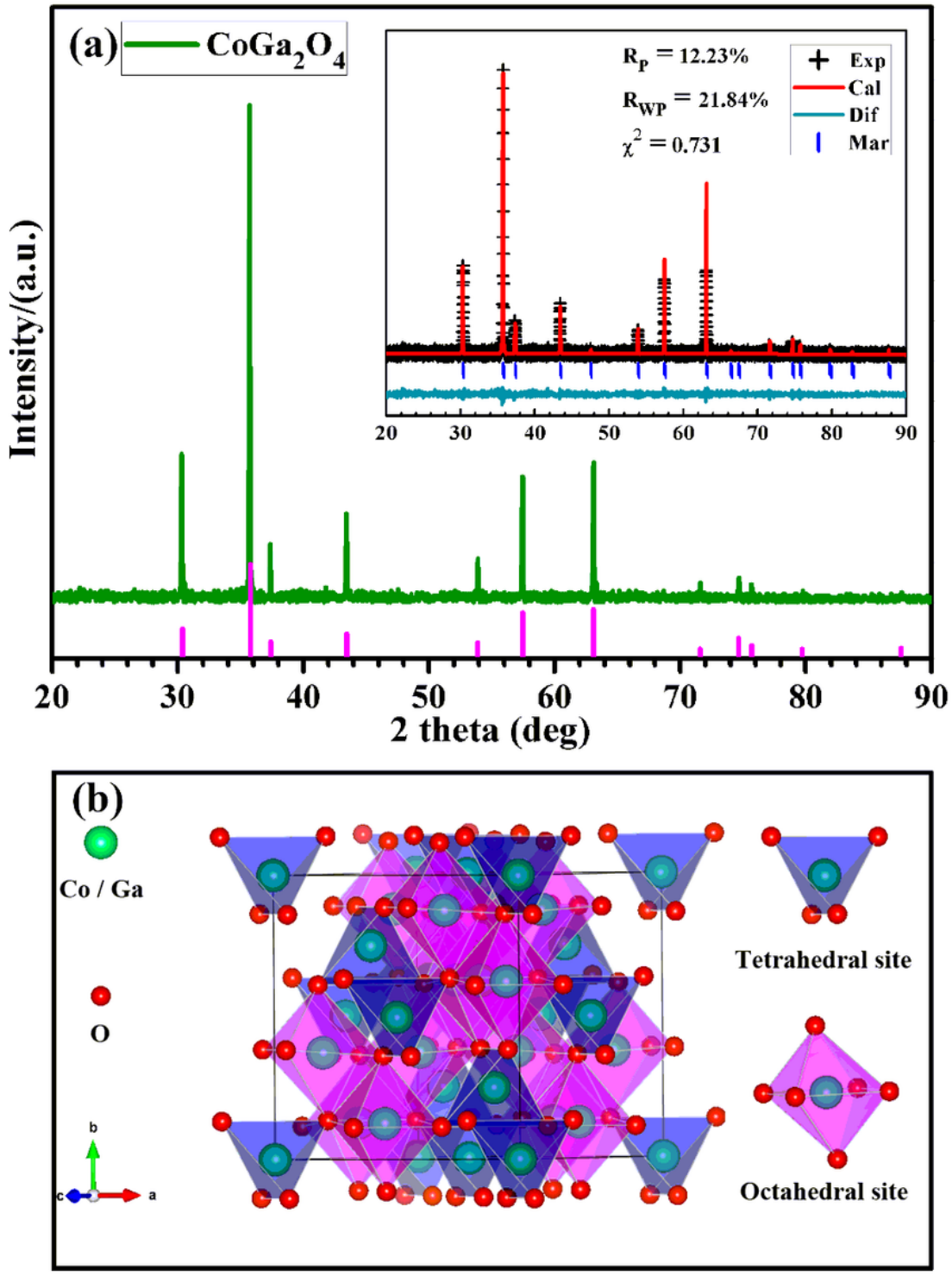

Figure 1

(a) XRD spectra and Rietveld refinement at room temperature for CoGa2O4. Inset shows the Rietveld refinement XRD pattern. (b) The crystal structure of CoGa2O4.

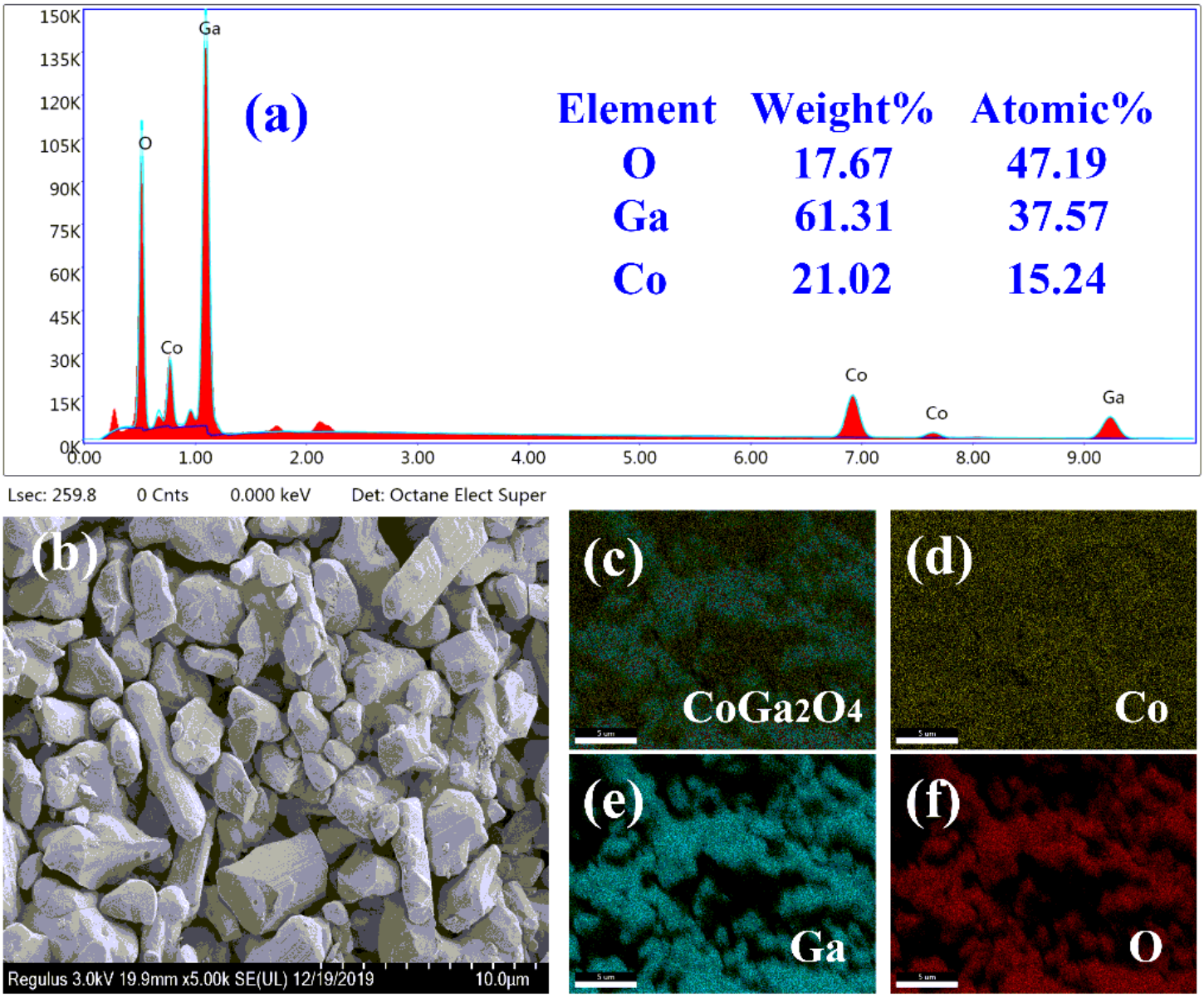

Figure 2

(a) EDX spectroscopy for the prepared sample. (b) SEM image of CoGa2O4. (c)-(f) EDX element maps for the sample.

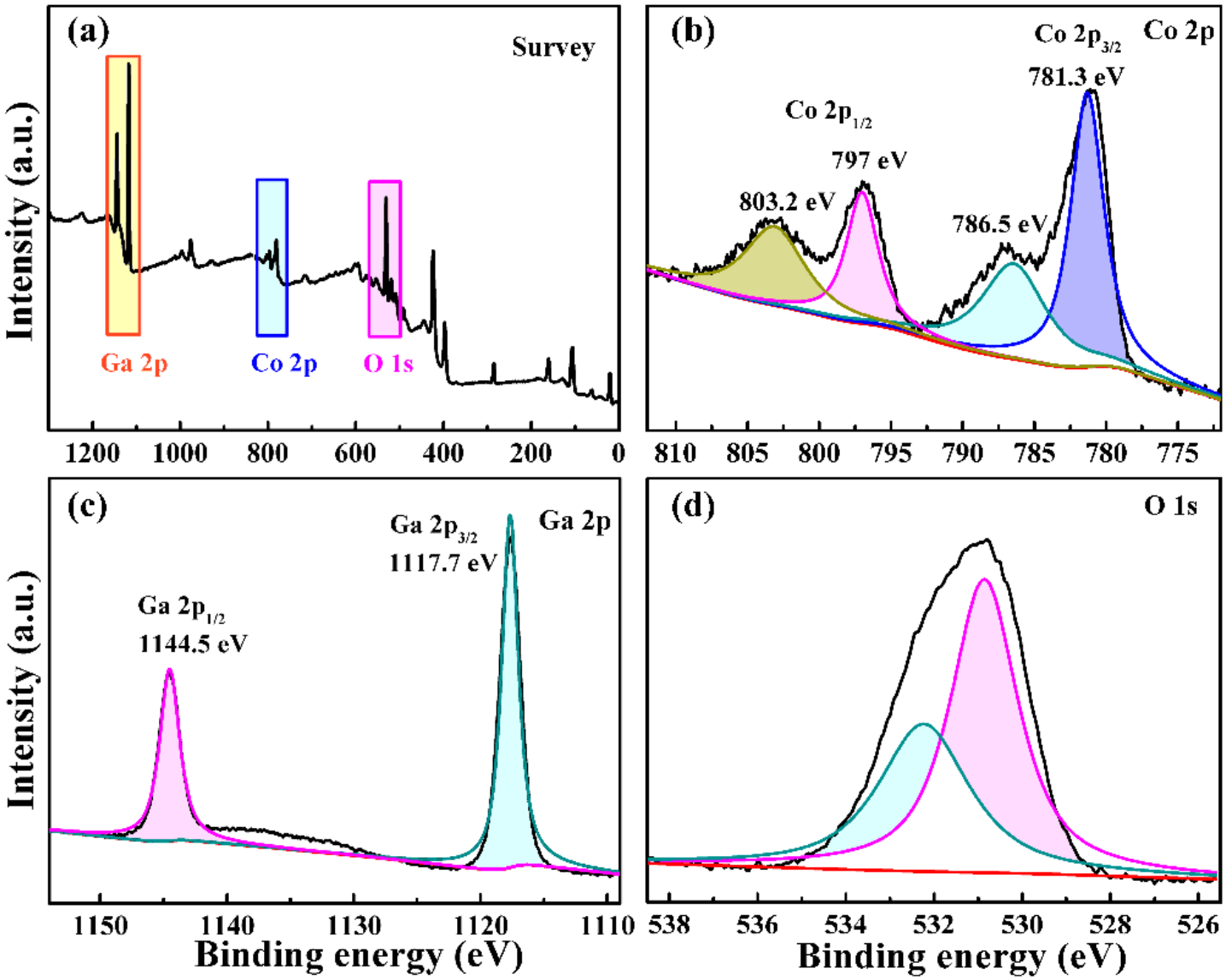

Figure 3

XPS spectrum of CoGa2O4: (a) The survey XPS spectra; (b) Co 2p; (c) Ga 2p; (d) O 1s.

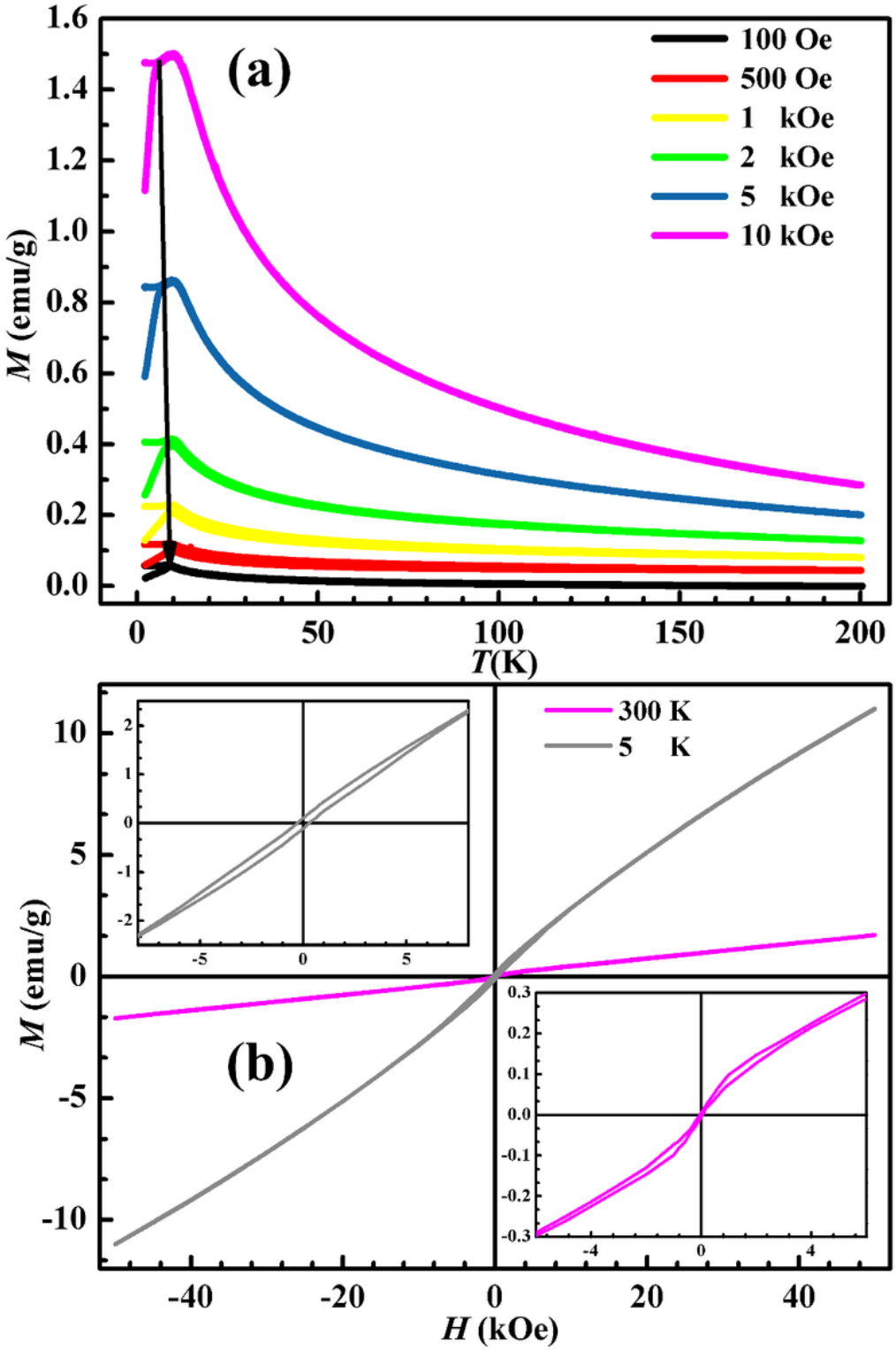

Figure 4

(a) M(T) curves for CoGa2O4 under ZFC/FC processes with different applied magnetic fields. (b) Magnetic hysteresis loops of CoGa2O4 at 5 and 300 K. The above and below insets show the enlarged M(H) region at 5 K and 300 K respectively.

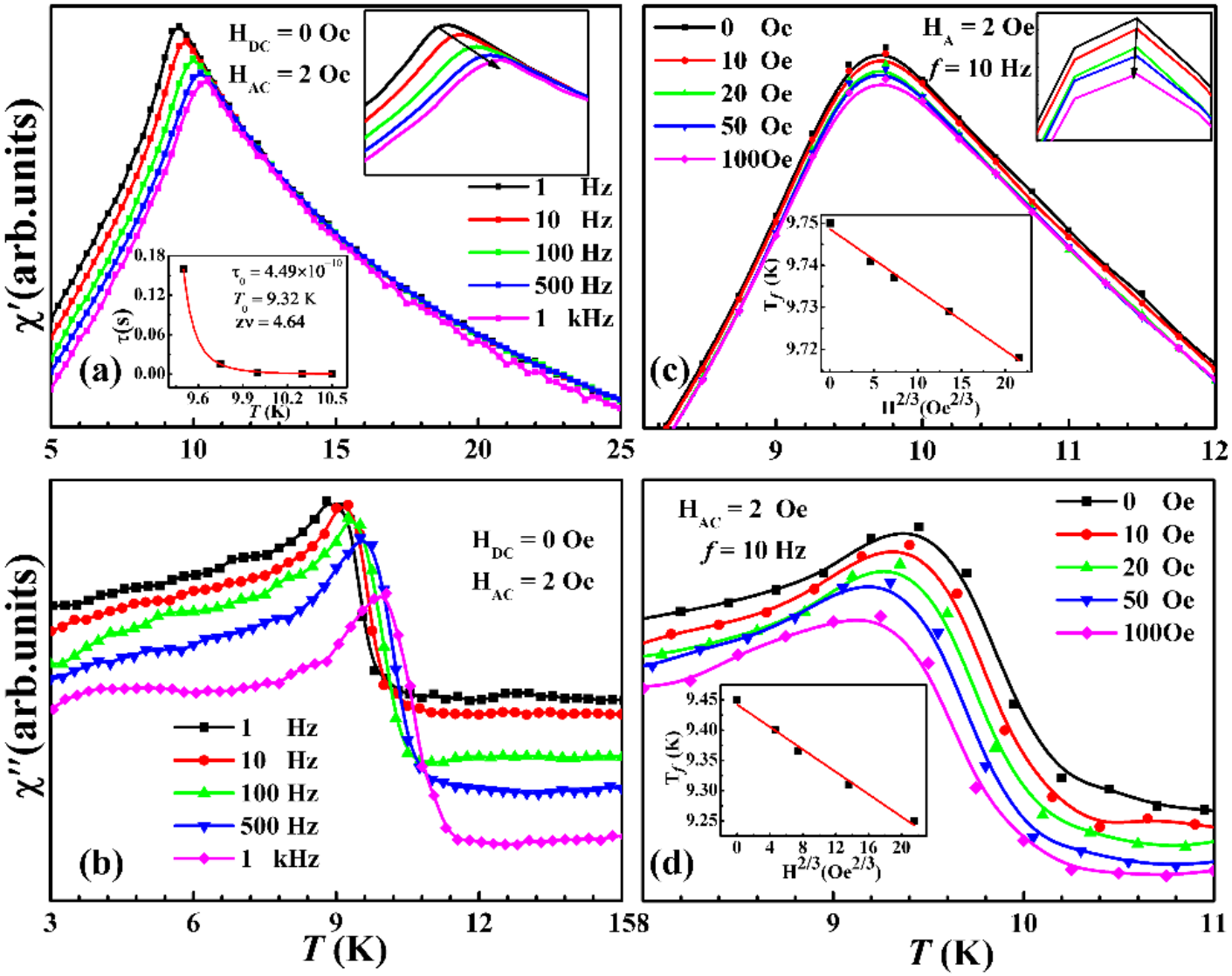

Figure 5

(a) and (b) Temperature dependence of χ'(T) and χ"(T) measured at several fixed frequencies for CoGa2O4. Inset of Fig. 5(a) stands for τ(s) vs T(K) plot. (c) and (d) Temperature dependence of χ'(T) and χ"(T) at several fixed DC fields. Both insets of Fig. 5(c) and 5(d) show the Tf plot as a function of H2/3.

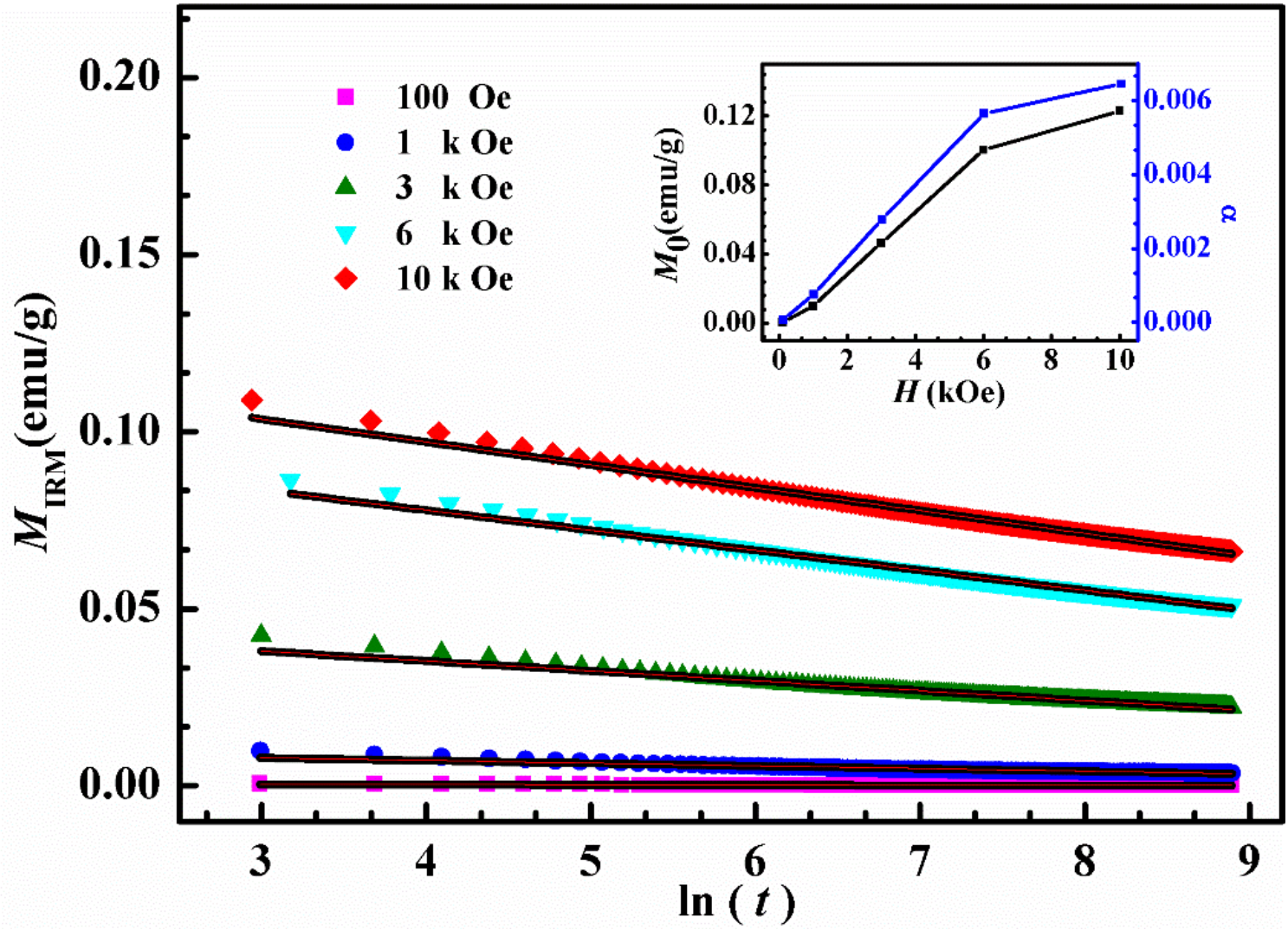

Figure 6

The plots of isothermal remanent magnetization (MIRM) at several fixed magnetic fields for CoGa2O4. The solid lines are obtained by fitting the experimental date with formula MIRM(t) = M0 – αln(t). The inset shows the magnetic field dependence fitting parameters M0 and α.

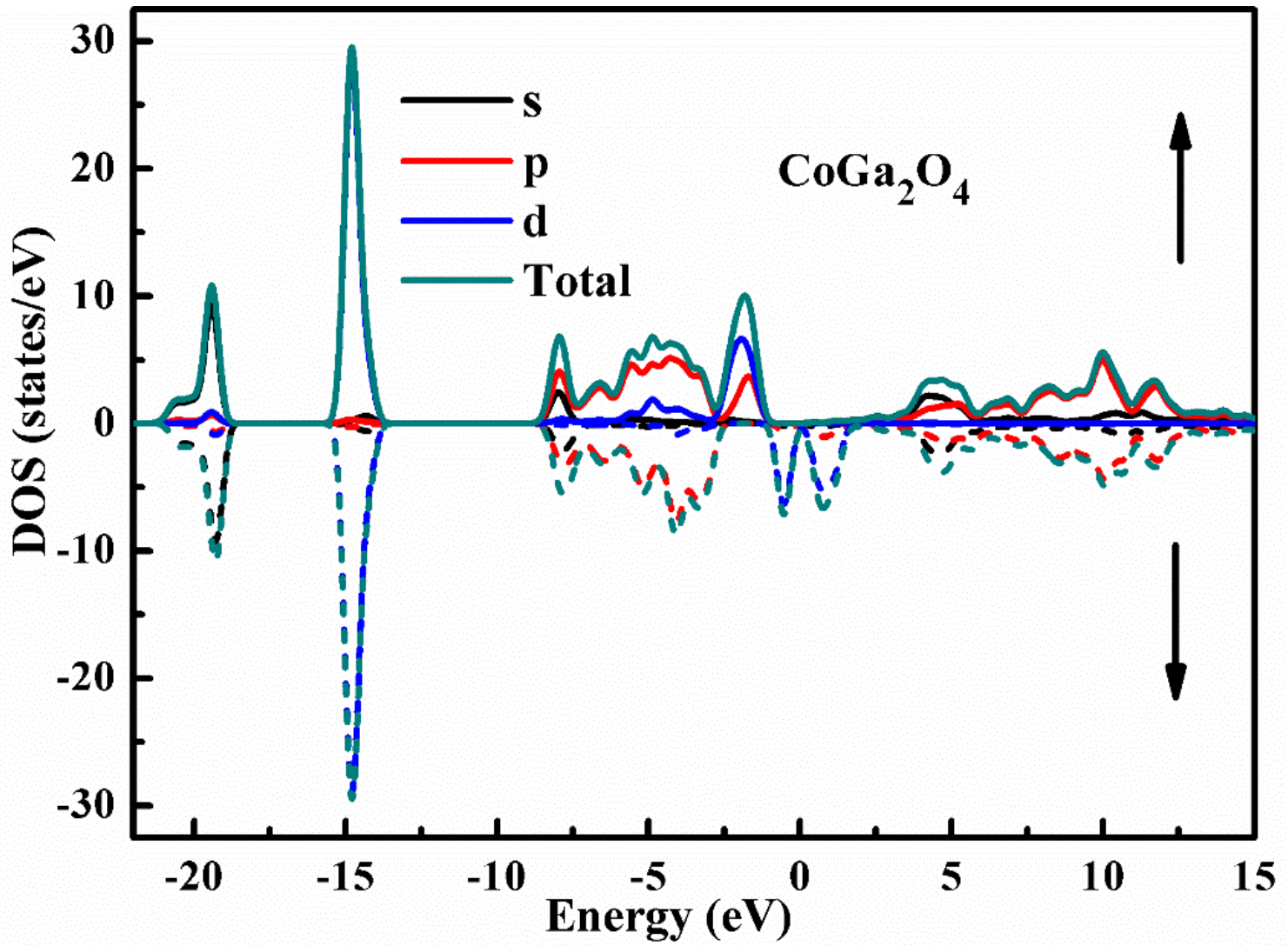

Figure 7

exhibited PODS and total DOS for spin-up (↑) and spin-down (↓) states for CoGa2O4 and the figure is formed by the s, p, d and Total states.